Extreme Mechanics Letters 8 (2016) 140–150

Contents lists available at ScienceDirect

Extreme Mechanics Letters

journal homepage: www.elsevier.com/locate/eml

Wedge-shaped twins and pseudoelasticity in fcc metallic nanowires under bending

Wolfram G. Nöhring [1], Johannes J. Möller, Zhuocheng Xie, Erik Bitzek *

Friedrich-Alexander-Universität Erlangen-Nürnberg, Department of Materials Science and Engineering, Institute I: General Materials Properties, Martensstr. 5, 91058 Erlangen, Germany

ARTICLE INFO

Article history:
Received 30 December 2015
Received in revised form 29 February 2016
Accepted 3 March 2016
Available online 27 April 2016

Keywords:
Nanowire
Bending
Twinning
Pseudoelasticity
Molecular dynamics

ABSTRACT

Molecular dynamics simulations were performed to study the deformation mechanisms of ⟨110⟩-oriented, faceted Cu and Au nanowires under bending along three different crystallographic directions. Independent of the bending direction, the stress field is characterized by a highly nonlinear elastic response, leading to a shift of the neutral fiber away from the central wire axis. The nanowires show ultra-high yield strengths, and the achievable large elastic strains directly influence the dislocation nucleation through the change of the unstable stacking fault energy. In agreement with theory and experiments on face-centered cubic ⟨110⟩ nanowires under uniaxial load, the tensile part of the wires exhibit deformation twinning, while plastic deformation in the compressed part takes place by slip of perfect dislocations. Independent of the bending direction, wire size, temperature and bending rate, all wires showed the formation of wedge-shaped twins. Upon instantaneous load removal, wires bent in two of the three directions showed spontaneous, pseudoelastic unbending. The findings of this study could be relevant for the design of flexible electronics and mechanical energy storage applications at the nanoscale.

1. Introduction

Metallic nanowires (NWs) have recently attracted a lot of attention due to their unique mechanical properties [1–4]. In particular defect free NWs, also sometimes referred to as nanowhiskers, are characterized by ultra-high yield strengths close to the theoretical strength, as dislocations have to be nucleated from the free surfaces [1,2,5]. For face-centered cubic (fcc) metals, such nucleation-controlled plasticity leads to a size and orientation dependence of the deformation mechanism [4,6,7]: whether full or partial dislocations are nucleated depends on the resolved shear stress on the leading an trailing partial dislocations as well as the stable and unstable stacking fault energies. Whether partial dislocations form a deformation twin depends furthermore on the unstable twinning energy. This theory successfully predicted the deformation of ⟨110⟩-oriented Au NWs by twinning under tension and by full dislocations in compression [7,8]. Deformation twinning of NWs was also predicted by molecular dynamics (MD) simulations to lead to pseudoelastic deformation and a shape memory effect [9–13], which was recently confirmed experimentally [8]. The high surface-to-volume ratio of NWs is furthermore believed to influence the elastic response of NWs through a combination of surface stress effects and nonlinear elastic response of the atoms within the strained core of the NW [4,9,14–16].

Most studies of metallic NWs to date have been performed under tensile testing conditions. Despite the importance of characterizing the deformation behavior under bending loads, e.g., for applications of metallic NWs in flexible and stretchable electronics [17–19], electronic and optoelectronic devices [20,21] or nano electromechanical

* Corresponding author.
E-mail address: erik.bitzek@fau.de (E. Bitzek).
[1] Now at: Laboratory for Multiscale Mechanics Modeling, École Polytechnique Fédérale de Lausanne, CH-1015 Lausanne, Switzerland.

http://dx.doi.org/10.1016/j.eml.2016.03.001

systems (NEMS) [22], only comparatively few NW bending experiments [14,23–30] and MD simulations [15,31–42] have been reported. In particular, the plastic deformation behavior during bending of [110]-oriented, faceted NWs typical for many fcc metals [5,7,8,43,44] has not yet been investigated in detail by atomistic simulations. According to [7,8], during bending these wires should show a competition between twinning in the part subjected to tensile stress and full dislocation slip in the compressive part of the NW.

Although Cai et al. have devised special bending periodic boundary conditions [33], these are not available in all MD codes, and various methods to apply bending loads or displacements are currently used throughout the literature. These include cantilever beams where forces are applied by an indenter [39], or directly on certain atoms [31,32], or the atoms at one end are rigidly displaced [15]; double-clamped wires where forces are applied by an indenter [36,38,45], or certain atoms are displaced with constant velocity [41]; by modeling four-point bending by applying forces to selected atoms [35]; by displacing all atoms according to a prescribed bending angle [40,46]; or by rotating fixed clamping regions [37]. Stress concentrations, e.g., due to the indenter or fixed clamping regions can however lead to unwanted dislocation nucleation.

In this letter, we report on MD simulations on ⟨110⟩-oriented Cu and Au NWs using a simple method to introduce bending loads without artificial stress concentrations. The ensuing stress field and deformation mechanisms are analyzed in detail for three different orientations of the wire with respect to the bending load.

2. Methods

Molecular dynamics (MD) simulations were performed on [01$\bar{1}$] oriented Cu and Au NWs with hexagonal cross-sections with two {100} and four {111} facets, see Fig. 1(a). This geometry is representative for many fcc NWs [5,7,8,43,44]. Three wires of different lengths l and diameters d were tested: a small wire (51 × 10 nm, 366,705 atoms), a large wire (102 × 20 nm, 2967,357 atoms) and a high-aspect ratio wire (102 × 10 nm, 732,505 atoms). Before performing the MD simulations, the wires were relaxed using the FIRE algorithm [47].

Bending moments were applied by imposing forces on atoms at the two ends of the wires, see Fig. 1(d). The magnitude of the force was increased linearly with time. The direction of the force was determined at each time step according to the cross-product between the bending axis (=z axis) and, for atoms in the left end of the wire (region 2), the vector connecting the center mass of region 2 to the center of mass of the wire center, region 1. Atoms in region 3 were given forces in the direction according to the cross-product between the bending axis and the vector connecting the center of mass of region 1 to center mass of region 2. The net momentum resulting by this approach was eliminated by subtracting from each atom the mean velocity vector. This procedure leads to stresses akin to a three-point bending test while avoiding artificial periodic boundary conditions and stress concentrations caused by an indenter or clamps. It allows also for the instantaneous

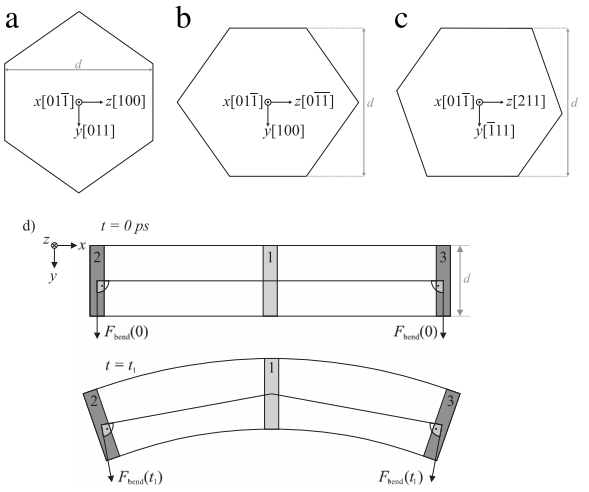

Fig. 1. Sketch of the wire cross-section (a–c) and simulation setup for the NW bending test (d). Three different orientations (a–c) with respect to the bending (z) axis were used to study the deformation of [01$\bar{1}$]-oriented NWs with hexagonal cross-sections. A bending moment was imposed by applying forces on the atoms in region 2 (3) in the direction of the cross-product between the bending axis and the vector connecting the centers of mass of regions 1 and 2 (the centers of mass of regions 3 and 1).

removal of the applied forces, which is important for the study of spontaneous, pseudoelastic, unbending. The widths of the regions were 1 nm, and forces were increased by $\dot{F}_{\text{bend}} = 300$ and 150 N/s.

Three orientations of the wire with respect to the bending axis were tested, see Fig. 1: (a) $z = [01\bar{1}], y = [100]$; (b) $z = [100], y = [011]$; (c) $z = [211], y = [\bar{1}11]$. While the first two configurations are mirror symmetric with respect to the plane normal to the bending axis, the cross-section of the last one has only point symmetry. In the following these configurations will be identified by the crystallographic direction along which the forces are applied ("bending direction", corresponding to the y-axis). MD simulations were performed in the microcanonical NVE ensemble with a starting temperature of 0 K and in the canonical NVT ensemble at 300 K, where the temperature was controlled with a Nosé–Hoover thermostat [48]. The temperature increase during the NVE simulations was in all cases below 50 K.

In addition to the bending simulations, the effect of unloading was simulated for the 51 × 10 nm Cu wires in all three orientations. In this case, the bending forces were instantaneously removed and the simulation was continued for 200 ps.

In the following, we characterize the deformation state by the displacement in y direction of the center of mass of the end regions, from which a nominal bending angle Θ^{nom} can be calculated under the assumption of an ideal Euler–Bernoulli beam. It has to be pointed out that this is only an approximate measure for the deformation, as the NWs do not represent ideal Euler–Bernoulli beams, and in particular in the case of local plastic deformation, no unique bending angle can be defined. As measure for the yield strength, we use the maximum nominal bending stress $\sigma_{B,\text{nom}}^{y,\max}$. It is a function of cross-section and orientation of the wire, see also the calculation of the area

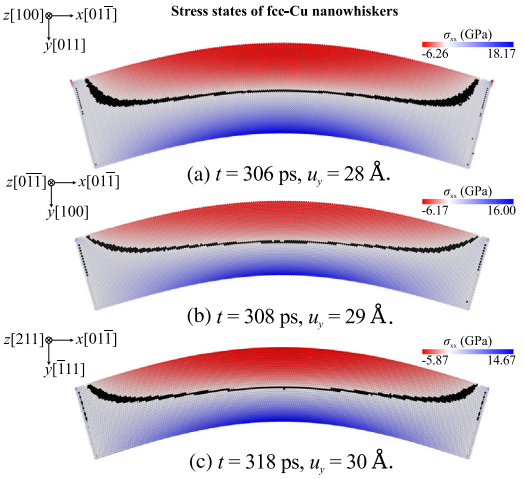

Fig. 2. Configuration and *xx*-component of the atomic stress tensor in the center of the 51 × 10 nm Cu wire directly before nucleation of the first dislocations in the NVE bending simulation with rate of force increase of $\dot{F}_{\text{bend}} = 300$ N/s; (a) [011] bending direction at $F_{\text{bend}} = 91.8$ nN ($\Theta^{\text{nom}} = 42°$); (b) [100] bending direction at $F_{\text{bend}} = 92.4$ nN ($\Theta^{\text{nom}} = 42°$); (c) [$\bar{1}$11] bending direction at $F_{\text{bend}} = 95.4$ nN ($\Theta^{\text{nom}} = 45°$). Please note the asymmetric color scales. Tensile stresses are negative, compressive stresses positive. Atoms with $|\sigma_{xx}| < 250$ MPa are colored black to highlight the neutral axis. Only non-surface atoms in a slice through the middle of the wire are shown. (For interpretation of the references to color in this figure legend, the reader is referred to the web version of this article.)

moments of inertia in the Supplementary Material, see Appendix A.

Embedded atom method (EAM) potentials were used to model the atomic interactions for Cu [49] and Au [50]. The simulations were carried out with the MD software package IMD [51]. The wires were visualized with AtomEye [52] and Ovito [53]. To detect dislocations, we used common neighbor analysis (CNA) [54], slip vector analysis [55] and the dislocation extraction algorithm (DXA) [56].

3. Results

Typical shapes of the elastically bent wires are shown in Fig. 2. Given the large strains attainable in the defect free NWs, the elastic response is non-linear, leading to compressive stresses which are two- to three times larger than the tensile stresses. The neutral axis is correspondingly shifted to the compressive region so that the wire is in equilibrium [57].

In all wires, plastic deformation was dominated by the formation of twins, although some full dislocation activity in the compressive part was observed in some cases. Table 1 summarizes the different simulations. In addition to the applied force $F_{\text{bend}}^{\text{y}}$ and time t^{y} at which yield occurred, also the corresponding nominal bending angle $\Theta_{\text{i}}^{\text{nom}}$, maximum bending moment $M_{\text{z}}^{\text{y,max}}$ and maximum nominal bending stress $\sigma_{B,\text{nom}}^{\text{y,max}}$ are provided using the area moments of inertia, Eqs. (4–6) given in the Supplementary Material, see Appendix A. Very high nominal yield stresses $\sigma_{B,\text{nom}}^{\text{y,max}}$ up to 18 GPa are obtained in the NVE simulations, however, at 300 K or with a lower rate $\dot{F}_{\text{bend}}$ these are reduced to 12–14 GPa.

A striking characteristic of *all* bending simulations was the formation of *wedge-shaped twins*. In the following, the morphology and deformation processes will be described in detail for the different bending orientations, using the results from the NVE simulations on small Cu wires and $\dot{F}_{\text{bend}} = 300$ N/s. The resulting structures are shown in Fig. 3 together with the Thompson tetrahedron showing the relative orientation of the slip systems. In general, the key features of the deformation processes were not significantly influenced by the material or simulation parameters. A summary of the results on Au NWs and snapshots from the other simulations are provided in the Supplementary Material, see Appendix A.

3.1. [011] *bending direction*

Fig. 3(a) shows the [011]-oriented wire at $F_{\text{bend}} = 95.4$ nN ($\Theta^{\text{nom}} = 47°$). Two wedge-shaped twins on the (c) and (a) planes (in Thompson tetrahedron notation [58]) can be clearly identified in the tensile region by the change of coordination number reflecting the crystallographic reorientation. Both twins appear to intersect in the middle (100) plane of the wire and display steps on the twin boundaries (TBs). The individual processes leading to this configuration are shown in Fig. 4(a), and the Supplementary Movies M1 and M2, see Appendix A. The twins were formed by multiple $\gamma A(c)$ and $C\alpha(a)$ partial dislocations which nucleated on adjacent planes at the top surface, see Fig. 4(a.i) and (a.ii). The first partial dislocations in each group stopped near the neutral axis while the others formed a pile-up like configuration, leading to the wedge-shaped twin configuration. The partial dislocations are stored in the TBs where they form the stepped structure. In the following, we refer to wedge-shaped twins where the twinning partial dislocations are stored in the TB as type-I twinning wedge (TW-I).

The situation was not ideally symmetric, since more $C\alpha(a)$ than $\gamma A(c)$ partial dislocations nucleated, and therefore one twin was larger than the other, see subfigure 4(a.iii). At the intersection of the twins, dislocation locks of type $C\gamma/A\alpha$ were formed, see Supplementary Material, Appendix A.

With increasing bending force, some partial dislocations $C\alpha(a)$ changed their glide plane to the (b) plane according to the dislocation reaction

$$C\alpha(a) \rightarrow C\beta(b) + \beta\alpha, \tag{1}$$

see Fig. 36a in the Supplementary Material, Appendix A. This reaction corresponds to the first step in the cross-slip process through an acute angle according to the Fleischer mechanism [59], which has also been observed in other simulations of nanostructured materials [60]. This process took also place at the twin on the (c) plane. There, the dislocations glided in the negative x direction, forming again an acute angle with the initial glide plane.

Only at later stages dislocation nucleated at the compressive side of the wire. However, the deformation was clearly more pronounced in the upper, tensile, part of the wire. Wires of different sizes show the same mechanisms and twin morphologies, however, not as symmetric as in Fig. 3(a), and one twin family could dominate, see Figure

Table 1
Summary of bending simulations on Cu NWs; t^{i}, $F^{\mathrm{i}}_{\mathrm{bend}}$ and $\Theta^{\mathrm{nom}}_{\mathrm{i}}$ denote the time, the bending force and the nominal bending angle when plastic deformation initiated; the corresponding maximum bending moment $M^{\mathrm{i,max}}_{\mathrm{z}}$ and maximum nominal bending stress $\sigma^{y,\mathrm{max}}_{B,\mathrm{nom}}$ are obtained using Eqs. (2–3) given in the Supplementary Information, see Appendix A; the deformation mechanism was either the formation of a type-I twinning wedge (TW-I) or the formation of a type-II twinning wedge (TW-II), see the text for detailed description of these mechanisms. For selected simulations, the maximum resolved shear stresses τ^{max} on leading (subscript 'lp') and trailing partial dislocations (subscript 'tp') in the compressive (subscript 'C') and tensile (subscript 'T') parts of the wire were calculated from the atomistic stress tensor of the configuration before dislocation nucleation, see Fig. 2.

Length l (nm)	Diameter d (nm)	$\dot{F}_{\mathrm{bend}}$ (N/s)	T (K)	t^{i} (ps)	$F^{\mathrm{i}}_{\mathrm{bend}}$ (nN)	$\Theta^{\mathrm{nom}}_{\mathrm{i}}$ (°)	$M^{\mathrm{i,max}}_{\mathrm{z}}$ (nN nm)	$\sigma^{y,\mathrm{max}}_{B,\mathrm{nom}}$ (GPa)	Mechanism	$\tau^{\mathrm{max}}_{\mathrm{C,lp}}$ (GPa)	$\tau^{\mathrm{max}}_{\mathrm{C,tp}}$ (GPa)	$\tau^{\mathrm{max}}_{\mathrm{T,lp}}$ (GPa)	$\tau^{\mathrm{max}}_{\mathrm{T,tp}}$ (GPa)
[011] bending direction													
51	10	300	0	308	92.5	42.68	2,314	16.9	TW-I	4.2	8.5	3.0	1.5
51	10	300	300	218	65.4	30.77	1,643	12.0	TW-I				
[100] bending direction													
51	10	300	0	310	93.1	43.41	2,336	16.1	TW-II	5.9	8.4	2.7	1.4
51	10	300	300	232	70.2	34.23	1,766	12.2	TW-II				
102	10	300	0	168	50.4	90.53	2,524	17.4	TW-II				
102	10	150	0	280	42.0	81.77	2,106	14.5	TW-II				
102	20	300	0	1242	372.6	42.21	18,764	16.2	TW-II				
[$\bar{1}$11] bending direction													
51	10	300	0	320	96.1	45.44	2,407	17.0	TW-I	3.3	6.8	3.5	2.5
51	10	300	300	234	70.2	34.79	1,790	12.7	TW-I				
102	10	300	0	170	51.0	90.22	2,553	18.0	TW-I				
102	10	150	0	330	49.5	85.77	2,479	17.5	TW-I				
102	20	300	0	1230	369.0	40.93	18,542	16.4	TW-I				

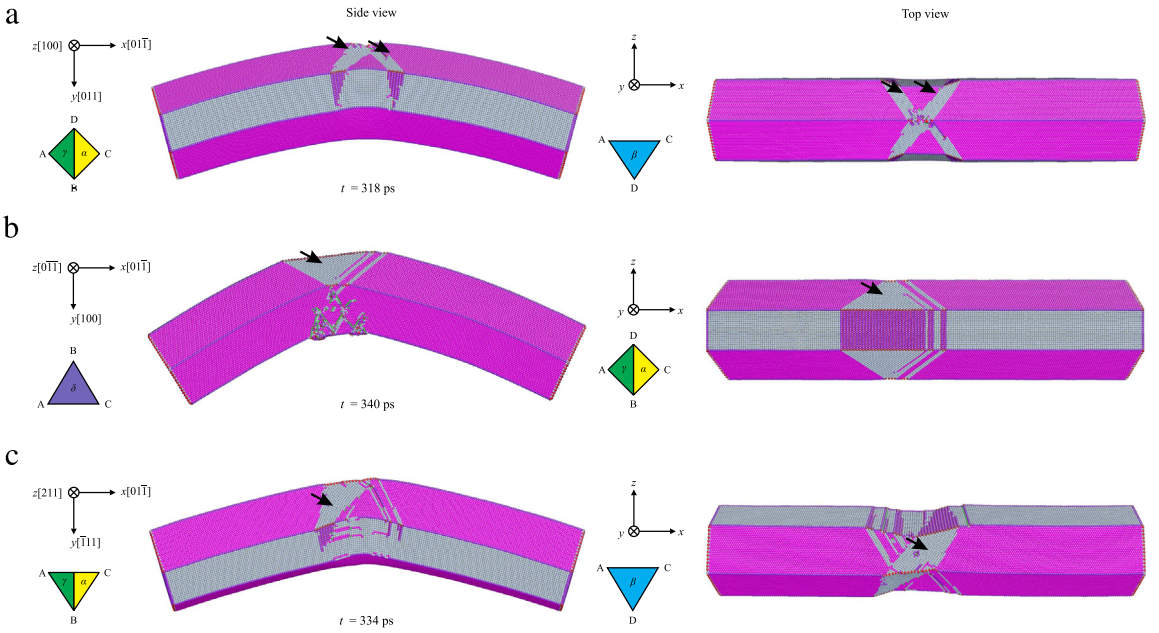

Fig. 3. Outside view on the 51 × 10 nm Cu wires after significant plastic deformation. The color coding represents the coordination number and can be used to identify {111} planes (pink) and {100} planes (grey). The orientation of the slip systems are indicated by Thompson tetrahedra. Arrows show the location of the wedge shaped twins, which change the crystallographic orientation of the surfaces. In the [011] bending direction (a), two intersecting twins are formed on the (a) and (c) planes, on which the twinning partial dislocations can be discerned (type-I twinning wedge). Upon bending along the [011] direction (b), only one, nearly mirror-symmetric twin was formed, without leaving any visible twinning dislocations on the TBs (type-II twinning wedge). Bending in [$\bar{1}$11] direction (c) lead to the formation of a dominant single type-I twinning wedge. (For interpretation of the references to color in this figure legend, the reader is referred to the web version of this article.)

19 in the Supplementary Material, Appendix A. At 300 K, the dislocation nucleation started earlier, see Table 1, and more twins were formed, see Movies M13 and M14. Similar to the Au wires, the key features, however, remained unchanged, see the Supplementary Material, Appendix A.

3.2. [100] *bending direction*

Fig. 3(b) shows the wedge-shaped twin that formed during bending in the [100] direction ($F_{\mathrm{bend}} = 102$ nN and $\Theta^{\mathrm{nom}} = 83°$). In contrast to Fig. 3(a), only one twin

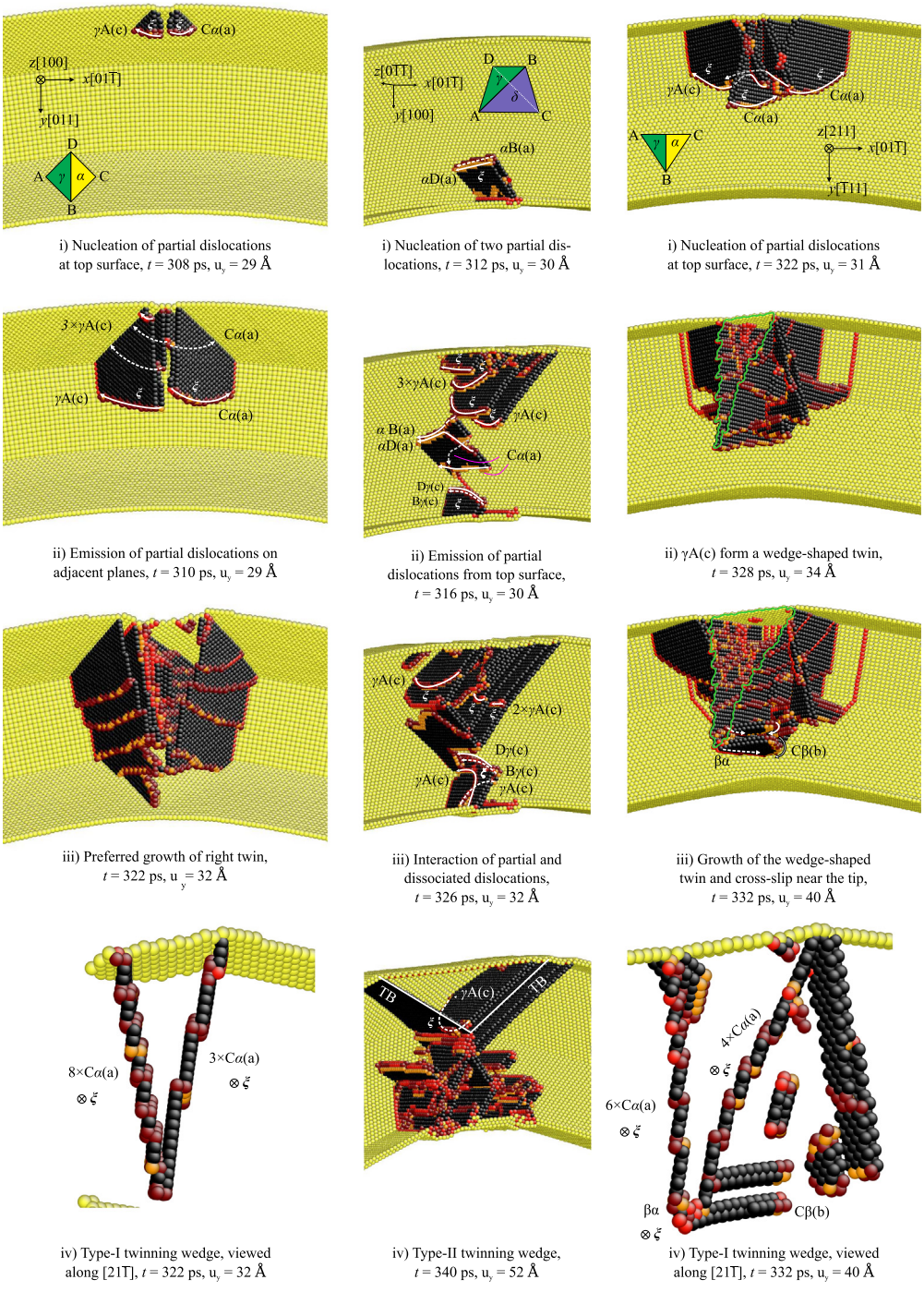

Fig. 4. Processes during the bending of a 51 × 10 nm Cu wire in different directions (a–c). The Thompson tetrahedra show the relative orientation of the slip systems. Atoms are colored according to the common neighbor analysis (yellow = surfaces, black = fcc stacking faults, orange and red = atoms in dislocation cores and other defects, atoms in perfect fcc stacking are not shown). The dislocations are characterized using the Thompson tetrahedron notation [58] for their Burgers vector, and white arrows indicate the line direction $\vec{\xi}$. Green lines in c.ii and c.iii are guides to the eye to delineate the wedge-shaped twin. Please note the different viewing directions in subfigures a.iv and c.iv. (For interpretation of the references to color in this figure legend, the reader is referred to the web version of this article.)

is formed, which is bounded by two flat TBs on the (a) and (c) planes. Such twins with flat TBs belonging to different faces of the Thompson tetrahedron will in the following be referred to as type-II twinning wedge (TW-II).

The processes leading to this configuration are described in detail in Fig. 4(b), and can be observed in the Supplementary Movies M3 and M4, see Appendix A. Plastic deformation started at a bending force of 93 nN ($\Theta^{\text{nom}} = 43°$). Two partial dislocations, $\alpha B(a)$ and $\alpha D(a)$, nucleated simultaneously on adjacent (111) planes at the bottom of the wire, see Fig. 4(b.i). They were immediately followed by the corresponding $C\alpha(a)$ trailing partial dislocations (Fig. 4(b.ii)), and the perfect dislocations $\alpha B(a) + C\alpha(a)$ ($=CB(a)$) and $\alpha D(a) + C\alpha(a)$ ($=CD(a)$) moved towards the neutral axis.

Soon after the nucleation of the dislocations in the compressive part of the wire, a number of $\gamma A(c)$ leading partial dislocations were nucleated at the top surface under tensile strain, some of them on adjacent planes, see Fig. 4(b.ii). They moved towards the center of the wire, where they interacted with the stacking fault ribbon formed by the dissociated $CB(a)$ and $CD(a)$ (Fig. 4(b.iii)). Subsequently, more $\gamma A(c)$ partial dislocations nucleated at the top surface. Some of the $\gamma A(c)$ partial dislocations slipped on (c) planes adjacent to stacking faults left by other partial dislocations with identical Burgers vector, thus creating microtwins. One of these TBs formed the right flank of what becomes the wedge-shaped twin, see Fig. 4(b.iv). Also some $C\alpha(a)$ dislocations were nucleated from the top surface. The interaction of the $\gamma A(c)$ partial dislocations with these partial dislocations on the (a) plane led to the left flank of the wedge-shaped twin. Exactly the same wedge-shaped twin formed in Cu wires of different sizes, bent at slower rates and at 300 K (movies M15 and M16), as well as in the Au wires at 0 and 300 K, see the Supplementary Material Appendix A.

While the wedge-shaped twin was formed at the top, a complicated, interlocked dislocation network formed at the bottom. In contrast to the top, trailing partial dislocations were frequently seen, and full dislocation slip on the (c) and (a) plane was observed (Fig. 4(b.iii)). It is important to note that both Burgers vectors with resolved shear stresses on the slip planes were activated, e.g. as well $CD(a)$ as $CB(a)$ were nucleated. Small twinned cells were formed where the bottom-nucleated dislocations slipped on adjacent planes. However, no single coherent twin region was created. The formation of dislocation locks along the $[0\bar{1}\bar{1}]$ axis, which is also the bending axis in this configuration, could frequently be observed.

3.3. $[\bar{1}11]$ bending direction

Fig. 3(c) shows the Cu wire during bending in the $[\bar{1}11]$ direction at $F_{\text{bend}} = 100.2$ nN ($\Theta^{\text{nom}} = 54°$). One large TW-I wedge-shaped twin with TBs on the (a) plane can be clearly identified. Longer wires, also tested at different bending rates, showed the same wedge-shaped twin morphology, however, with twins on the (a) and (c) system, see Figs. 27 and 28 in the Supplementary Material, Appendix A.

The processes leading to the formation of the twin in Fig. 3(c) are shown in Fig. 4(c), and Supplementary Movies M5 and M6, see Appendix A. The twin was formed by $C\alpha(a)$ partial dislocations, which were nucleated at the top of the wire in the region of tensile stress. Some partial dislocations $\gamma A(c)$ were nucleated together with the first $C\alpha(a)$. However, the $\gamma A(c)$ did not form a complete wedge-shaped twin, because the twin formed by the $C\alpha(a)$ partial dislocation intersects their slip plane and blocked them. Only a few dislocations on the (c) plane managed to intersect the twin on the (a) plane. While some trailing partial dislocations ($D\gamma(c)$, $B\gamma(c)$ and $\alpha D(a)$) nucleated at the top in this case, almost no dislocation activity took place at the bottom of the wire. The mechanisms are very similar to the [011] bending direction, and again, partial dislocations forming steps on the TBs changed their glide plane to the (b) plane according to the first step of the Fleischer mechanism for cross-slip through an acute angle, see Fig. 4(c.iv) and Fig. 36b of the Supplementary Material. The same types of twins and processes are observed at 300 K (movies M17 and M18) and in the Au NWs, see the Supplementary Material, Appendix A.

3.4. Behavior after load removal

To test whether the bent wires would show pseudoelastic behavior, the applied bending forces on the 51 × 10 nm Cu NWs were instantaneously removed and the evolution of the wire was followed for 200 ps, for both, the simulation performed in the NVE as well as in the NVT ensemble at 300 K. The starting configurations for the three orientations (a–c) are shown in the left part of the subfigures in Fig. 5. The time, or respective bending angle, at which the force was removed was chosen such that the wedge-shaped twins were fully formed, but no massive dislocation reactions have taken place. For the NVE simulations in the [110] orientation, the force was removed at a nominal bending angle of $\Theta^{\text{nom}} = 56°$, for the [100] bending direction, the load was removed at a nominal bending angle of $\Theta^{\text{nom}} = 83°$, and in case of [111] at $\Theta^{\text{nom}} = 49°$. The corresponding nominal bending angles in the 300 K simulations were $\Theta^{\text{nom}}([110]) = 64°$, $\Theta^{\text{nom}}([100]) = 75°$ and $\Theta^{\text{nom}}([111]) = 55°$.

The evolution of the wire shape and defect content is shown in movies M7–M12 (NVE) and M19–M24 (300 K) in the Supplementary Material, see Appendix A. The configurations 200 ps after load removal are shown in the right part of the subfigures in Fig. 5. It can be clearly seen that wires that plastically accommodated the bending by the formation of TW-I twinning wedges regained a straight shape, whereas the wire with the flat TW-II wedge-shaped twin remained plastically bent.

Due to the inertia of dislocations [58,61] and the time for elastic waves to travel through the wire, the motion of the dislocations was not instantaneously stopped or reversed once the bending forces were removed, but the wires continued to deform for a short period of time in the initial direction. For the wire bent in [011] direction, Fig. 5(a), the twinning dislocations stored in the outer boundaries of the twins started to move back to the upper surface once the ends of the wire started to move up due

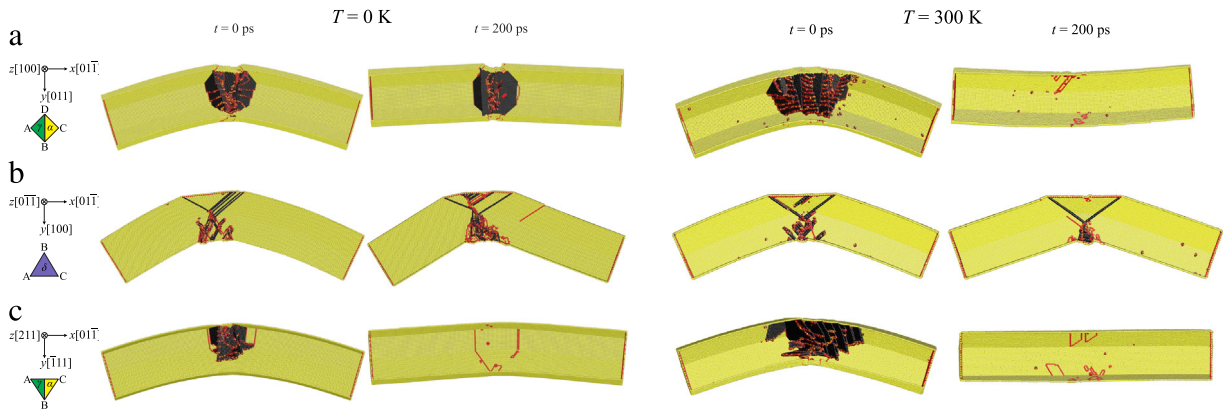

Fig. 5. Dislocation and twin structures in the interior of the 51 × 10 nm Cu wires before instantaneous removal of the bending forces and 200 ps after for the NVE simulations (left) and the NVT simulations at 300 K (right). (a) [011]; (b) [100] and (c) [$\bar{1}$11] bending direction. See Fig. 4 for the color code. (For interpretation of the references to color in this figure legend, the reader is referred to the web version of this article.)

to the stored elastic energy, and twinning dislocations on the inner TBs moved further down, leading to relatively straight twins passing through the entire wire. The initial intersection of the twins led to some remaining complex dislocation structure in the case of the NVE simulation, as shown on the right side of the left subfigure in Fig. 5(a). In the 300 K simulations, plastic deformation started earlier (see Table 1) and less energy is stored in the elastic bending of the wire. The deformation at 300 K is also generally less localized than in the 0 K simulations. This might contribute to fewer irreversible dislocation reactions for the 300 K simulation and consequently the complete removal of dislocations from the wire upon unbending, as can be seen in on the right side of Fig. 5(a).

Unloading of the Cu wires bent in [100] led to lots of dislocation activity in the lower, compressive parts of the wires, which resulted in complex, also roughly wedge-shaped patterns of dislocation locks, see Fig. 5(b). In both, the 300 K and NVE simulations, the wedge-shaped twins in the tensile regions grew slightly while the ends of the wires still moved down. Once the wire ends moved up again, a secondary wedge shaped twin formed inside the first twin in case of the NVE simulation, see the left subfigure of Fig. 5(b).

Upon removing the bending forces in the NVE simulation of the wire oriented in [$\bar{1}$11] direction, the dominant wedge-shaped twin transformed first into a twin with parallel TBs transecting the entire wire by the escape of the twinning partial dislocation through the lower surface of the wire. The wire then elastically bent in the opposite direction, which led to a wedge-shaped twin of opposite orientation by the nucleation of partial dislocations of opposite sign on the top surface. At the end, detwinning was complete, and the wire was free of any dislocations or twins, see the left subfigure of Fig. 5(c). In the bending simulation at 300 K, multiple wedge shaped twins formed on the same twin system, which upon unloading all moved back. Only one thin transecting planar twin and few thin wedge-shaped twins were formed while the wire bent in the opposite direction, and they all retracted, leaving a dislocation and twin free wire, see the right subfigure of Fig. 5(c). These simulations thus demonstrate clear pseudoelastic behavior of bent NWs with TW-II twins, both at 0 and 300 K.

4. Discussion

Single-crystalline, defect-free metallic nanowires or nanowhiskers are well-known to exhibit very large yield stresses, up to many GPa, when tested in tension [1–3,5,7,43,44,62]. The large strains thus possible in tension were shown experimentally to lead to nonlinear elastic response [44]. Under bending, similar or even larger stresses and strains are expected and measured also under experimental conditions [23,28,63]. The nonlinear elastic material response is a direct consequence of the non-linearity of the atomic bonding. For the employed Cu potential, this is illustrated in Fig. 6(a), using the effective pair potential formalism [64]. Nonlinear elasticity, in particular the increase of the Young's modulus in compression and a decrease in tension for [110] oriented crystals [9,16,44] and the subsequent shift of the neutral axis from the centroidal axis of the wire, should therefore be considered when analyzing experiments on NW bending or in the design of flexible electronics [17,19] or nano electromechanical systems (NEMS) [22]. A corresponding analytical framework for cantilever beams based on the generalized Ludwick constitutive law has been recently developed [57,65,66]. Given that the neutral axis of bent NWs can deviate from the wire center, simulation methods which assume or enforce a certain position of the neutral layer [35,46] might lead to artifacts.

It needs to be pointed out that the nonlinear elastic response due to large strains attainable in bending of NWs acts in addition to the size-dependent nonlinear elasticity of NWs [4,9,16]. For small diameters, the surface stresses have been shown to lead to a compressive strain in [110] oriented NWs, which in turn lead to an increase in the Young's modulus. For the present Cu NWs, the increase is however below 5% [16], and the average stress within the relaxed straight 51 × 10 nm NW is $\sigma_{xx} = -0.46$ GPa. Surface or size effects can thus not explain the factor of two differences in magnitude of the stresses between the tensile and compressive side in Fig. 3.

Given the very high stresses in the compressed side of the NWs, it is remarkable that most dislocations are nucleated on the tensile side of the wire, and only in the [100]

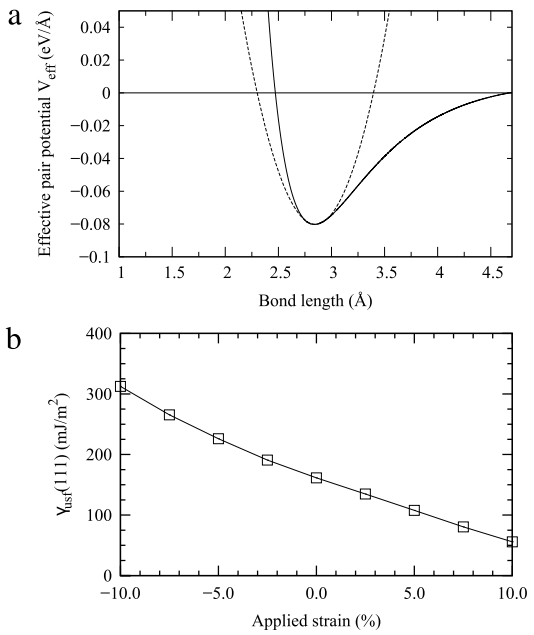

Fig. 6. (a) Effective pair potential for Cu [49,64]. The dashed line represents a parabolic fit around the minimum, illustrating the nonlinearity of the potential for large strains. Please note, that in the effective pair potential formalism, the minimum of the effective pair potential does not correspond to the equilibrium nearest-neighbor distance in an fcc lattice [64]. (b) Unstable stacking fault energy of the Cu potential [49] as a function of strain normal to the glide plane, calculated from static simulations allowing for Poisson contraction.

orientation plasticity is initiated by the nucleation of dislocations in the compressive part of the NW. Also the maximal resolved shear stress $\tau^{\max}$ calculated from the atomic stress tensor before the onset of plasticity is significantly larger for leading partial dislocations nucleated in the compressive part than in the tensile part, at least in the case of bending in the [011] and [100] directions, see Table 1. However, even in the [011] orientation, dislocation nucleation took place only in the tensile part of the wire. Dislocation nucleation does, however, not only depend on the resolved shear stress, but also on the height of the energy barrier which needs to be overcome to nucleate a leading partial dislocation. The nucleation barrier can be related to the unstable stacking fault energy γ_{usf} [67]. This quantity also depends on the lattice strain, and for the strain values before dislocation nucleation, the potential in this study shows a more than five times lower γ_{usf} in tension than in compression, see Fig. 6(b). Like in the case of tension–shear coupling for dislocation nucleation in the highly stressed region around a crack tip [67,68], the high tensile strains on the upper surface of the bend wire reduce the critical stress for the nucleation of a leading partial dislocation.

The mechanisms of deformation – twinning in the tensile part and full dislocation slip in the compressive part – are consistent with theoretical considerations regarding the active deformation mode, see e.g. [4,7,69] and experimental observations on [110] oriented fcc NW, which show twinning under tension [7,8] and full dislocation slip in compression [8].

Provided that twinning is the dominating deformation mechanism in the tensile part of the wire, the occurrence of wedge-shaped twins is a natural consequence of the strain gradient due to the bending. The plastic accommodation of the strain gradient requires the formation of geometrically necessary dislocations (GNDs). In nucleation controlled plasticity like in the case of defect free NWs, all GNDs need to be provided from the surface. The plastic strain gradient therefore can only result from the distance which the dislocations slip from the surface. The arrangement of the surface-nucleated partial dislocations into a wedge-shaped twin is the energetically most favorable arrangement of partial dislocations to accommodate the strain gradient. Accordingly, the wedge-shaped twins can be considered geometrically necessary twins (GNTs) [70]. Wedge-shaped GNTs should therefore be a general feature of [110] oriented, defect-free fcc NWs under bending, or more general, of bent nanostructures which deform dominantly by twinning. Indeed, all our simulations showed wedge-shaped GNTs, independent of size, aspect ratio, temperature and bending rate, see Appendix A. Wedge-shaped GNTs can also be identified in other atomistic simulations of bent NWs, although they were not specifically addressed as such [41].

The shape, size and location of the wedge-shaped GNTs will depend on the wire geometry and the details of the loading. Here, the TW-II wedge-shaped twins are a special case. They can only form if the bending axis lies within two glide planes with similar resolved shear stresses. As they do not contain any twinning dislocations on their TBs, these structures are relatively stable, and consequently, the plastic bending is not easily reversed, see Fig. 5(b).

Pseudoelasticity due to twinning/detwinning was already reported in atomistic simulations [10–13], and recently also observed experimentally [8]. In contrast to prior studies where pseudoelasticity of NWs was studied under displacement control in tension and compression [10–13], two of the NWs studied here in bending returned spontaneously to their straight shape once the load was removed (Fig. 5(a), (c)). The fact that pseudoelasticity was observed for NVE simulations starting at 0 K as well as for NVT simulations at 300 K and different nominal bending angles demonstrates the robustness of this phenomenon for [110] oriented NWs bent in [011] and [$\bar{1}$11] directions.

Key to the pseudoelastic behavior in this case was the storage of the twinning dislocations on the TBs of the TW-II wedge-shaped twins together with the comparatively few interactions between defects leading to few sessile dislocation locks. The spontaneous untwinning and return to the original shape is most probably caused additionally by the "spring-back" of the elastically loaded arms of the wire, see movies M7, M11, M19 and M23. This elastic unbending leads to a lever-type action on the central twin segment, providing an additional driving force for its untwinning. Such a lever-type action is not present under uniaxial loading. There, additional driving forces, e.g. by applying displacements in the opposite direction or surface stresses [12] are required for detwinning and the return to the original shape.

The simulations results reported here can of course not be directly applied to experimental conditions: the usual limitations in size and simulated times of MD simulations apply, leading to very fast bending rates, and the potential

might not correctly represent material properties like surface and stacking fault energies or elastic constants, in particular at the large strains in the present setup. However, key features of the simulations, like large yield stresses, twinning dominated plasticity under tension and full dislocations under compression and pseudoelastic behavior have been reported for uniaxial deformation in experiments [5,7,8,44]. Furthermore, the main outcomes of this study, namely the effect of large strains on elastic constants and subsequently the position of the neutral axis as well on the unstable stacking fault energy, and the preferred occurrence of wedge-shaped twins should only quantitatively but not qualitatively depend on the atomic interaction model, size, loading rates and setup. It is therefore suggested that wedge-shaped GNTs and pseudoelastic behavior should also be observable under typical experimental conditions.

In order to benefit from pseudoelastic behavior under bending, it is however important to minimize competing deformation mechanisms to the formation of wedge-shaped GNTs, e.g., dislocation nucleation by indentation or at stress concentrations (clamps). Furthermore, the formation of non-intersecting twin segments is desirable. Pseudoelastic buckling of adequately designed beams or bending of cantilever geometries could provide new possibilities to store mechanical energy in nanoscale devices.

5. Conclusions

We devised a simple setup to perform MD simulations of bending on [110]-oriented copper and gold nanowires in different directions. The large strains attainable in nanowires under bending lead to a pronounced nonlinear elastic response and a subsequent shift of the neutral layer from the central wire axis. In agreement with theory and experiments on uniaxially strained nanowires, the part of the wire under tension deforms by deformation twinning while plasticity in the compressed part of the wire takes place by slip of perfect dislocations. The dominance of twinning versus full dislocations could be traced to the significant decrease of the unstable stacking fault energy with tensile strain, thus leading to easier nucleation of partial dislocations in the tensile strained part of the wire compared to the compressed part. All wires, independent of size, temperature, rate and direction of bending showed the formation of geometrically necessary wedge-shaped twins. Spontaneous pseudoelastic unbending after instantaneous load removal was observed in two of the three bending orientations and can be explained by the storage of twinning dislocations in the twin boundaries of the wedge-shaped twins. The outcomes of this study could be relevant for the design of flexible electronics and mechanical energy storage applications at the nanoscale.

Acknowledgments

Z.X. gratefully acknowledges financial support from the German Science Foundation (DFG) via the research training group GRK 1896 “In Situ Microscopy with Electrons, X-rays and Scanning Probes”. We furthermore want to thank Ju Li and Daniel S. Gianola for fruitful discussions and Julien Guénolé for his help with some simulations.

Appendix A. Supplementary data

Supplementary material related to this article can be found online at http://dx.doi.org/10.1016/j.eml.2016.03.001.

References

[1] T. Zhu, J. Li, Ultra-strength materials, Prog. Mater. Sci. 55 (7) (2010) 710–757. http://dx.doi.org/10.1016/j.pmatsci.2010.04.001.
[2] O. Kraft, P.A. Gruber, R. Mönig, D. Weygand, Plasticity in confined dimensions, Annu. Rev. Mater. Res. 40 (1) (2010) 293–317. http://dx.doi.org/10.1146/annurev-matsci-082908-145409.
[3] J.R. Greer, J.T. De Hosson, Plasticity in small-sized metallic systems: Intrinsic versus extrinsic size effect, Prog. Mater. Sci. 56 (6) (2011) 654–724. http://dx.doi.org/10.1016/j.pmatsci.2011.01.005.
[4] C.R. Weinberger, W. Cai, Plasticity of metal nanowires, J. Mater. Chem. 22 (8) (2012) 3277. http://dx.doi.org/10.1039/c2jm13682a.
[5] L.Y. Chen, M.-r. He, J. Shin, G. Richter, D.S. Gianola, Measuring surface dislocation nucleation in defect-scarce nanostructures, Nature Mater. 14 (7) (2015) 707–713. http://dx.doi.org/10.1038/nmat4288.
[6] M. Chen, Deformation twinning in nanocrystalline aluminum, Science 300 (5623) (2003) 1275–1277. http://dx.doi.org/10.1126/science.1083727.
[7] A. Sedlmayr, E. Bitzek, D.S. Gianola, G. Richter, R. Mönig, O. Kraft, Existence of two twinning-mediated plastic deformation modes in Au nanowhiskers, Acta Mater. 60 (9) (2012) 3985–3993. http://dx.doi.org/10.1016/j.actamat.2012.03.018.
[8] S. Lee, J. Im, Y. Yoo, E. Bitzek, D. Kiener, G. Richter, B. Kim, S.H. Oh, Reversible cyclic deformation mechanism of gold nanowires by twinning–detwinning transition evidenced from in situ TEM, Nat. Commun. 5 (2014) http://dx.doi.org/10.1038/ncomms4033.
[9] W. Liang, M. Zhou, Pseudoelasticity of single crystalline Cu nanowires through reversible lattice reorientations, J. Eng. Mater. Technol. 127 (4) (2005) 423. http://dx.doi.org/10.1115/1.1928915.
[10] H.S. Park, K. Gall, J.A. Zimmerman, Shape memory and pseudoelasticity in metal nanowires, Phys. Rev. Lett. 95 (25) (2005) 255504. http://dx.doi.org/10.1103/PhysRevLett.95.255504.
[11] W. Liang, M. Zhou, Atomistic simulations reveal shape memory of FCC metal nanowires, Phys. Rev. B 73 (11) (2006) 115409. http://dx.doi.org/10.1103/PhysRevB.73.115409.
[12] X. Guo, W. Liang, M. Zhou, Mechanism for the pseudoelastic behavior of FCC shape memory nanowires, Exp. Mech. 49 (2) (2009) 183–190. http://dx.doi.org/10.1007/s11340-008-9173-x.
[13] C. Deng, F. Sansoz, A new form of pseudo-elasticity in small-scale nanotwinned gold, Extreme Mech. Lett. (2015) http://dx.doi.org/10.1016/j.eml.2015.12.004.
[14] G.Y. Jing, H.L. Duan, X.M. Sun, Z.S. Zhang, J. Xu, Y.D. Li, J.X. Wang, D.P. Yu, Surface effects on elastic properties of silver nanowires: Contact atomic-force microscopy, Phys. Rev. B 73 (23) (2006) 235409. http://dx.doi.org/10.1103/PhysRevB.73.235409.
[15] M.T. McDowell, A.M. Leach, K. Gall, Bending and tensile deformation of metallic nanowires, Modelling Simul. Mater. Sci. Eng. 16 (4) (2008) 045003. http://dx.doi.org/10.1088/0965-0393/16/4/045003.
[16] F. Niekiel, E. Spiecker, E. Bitzek, Influence of anisotropic elasticity on the mechanical properties of fivefold twinned nanowires, J. Mech. Phys. Solids 84 (2015) 358–379. http://dx.doi.org/10.1016/j.jmps.2015.08.004.
[17] L. Hu, H.S. Kim, J.-Y. Lee, P. Peumans, Y. Cui, Scalable coating and properties of transparent, flexible, silver nanowire electrodes, ACS Nano 4 (5) (2010) 2955–2963. http://dx.doi.org/10.1021/nn1005232.
[18] J.-W. Lim, D.-Y. Cho, K. Eun, S.-H. Choa, S.-I. Na, J. Kim, H.-K. Kim, Mechanical integrity of flexible Ag nanowire network electrodes coated on colorless PI substrates for flexible organic solar cells, Sol. Energy Mater. Sol. Cells 105 (2012) 69–76. http://dx.doi.org/10.1016/j.solmat.2012.05.036.
[19] S. Yao, Y. Zhu, Nanomaterial-enabled stretchable conductors: Strategies, materials and devices, Adv. Mater. 27 (9) (2015) 1480–1511. http://dx.doi.org/10.1002/adma.201404446.
[20] Y. Li, F. Qian, J. Xiang, C.M. Lieber, Nanowire electronic and optoelectronic devices, Mater. Today 9 (10) (2006) 18–27. http://dx.doi.org/10.1016/S1369-7021(06)71650-9.
[21] W. Wang, Q. Yang, F. Fan, H. Xu, Z.L. Wang, Light propagation in curved silver nanowire plasmonic waveguides, Nano Lett. 11 (4) (2011) 1603–1608. http://dx.doi.org/10.1021/nl104514m.

[22] A. Husain, J. Hone, H.W.C. Postma, X.M.H. Huang, T. Drake, M. Barbic, A. Scherer, M.L. Roukes, Nanowire-based very-high-frequency electromechanical resonator, Appl. Phys. Lett. 83 (6) (2003) 1240. http://dx.doi.org/10.1063/1.1601311.

[23] B. Wu, A. Heidelberg, J.J. Boland, Mechanical properties of ultrahigh-strength gold nanowires, Nature Mater. 4 (7) (2005) 525–529. http://dx.doi.org/10.1038/nmat1403.

[24] B. Wu, A. Heidelberg, J.J. Boland, J.E. Sader, Sun, Li, Microstructure-hardened silver nanowires, Nano Lett. 6 (3) (2006) 468–472. http://dx.doi.org/10.1021/nl052427f.

[25] L. Philippe, I. Peyrot, J. Michler, A.W. Hassel, S. Milenkovic, Yield stress of monocrystalline rhenium nanowires, Appl. Phys. Lett. 91 (11) (2007) 111919. http://dx.doi.org/10.1063/1.2785153.

[26] V. Cimalla, C.-C. Röhlig, J. Pezoldt, M. Niebelschütz, O. Ambacher, K. Brückner, M. Hein, J. Weber, S. Milenkovic, A.J. Smith, A.W. Hassel, Nanomechanics of single crystalline tungsten nanowires, J. Nanomater. 2008 (2008) 1–9. http://dx.doi.org/10.1155/2008/638947.

[27] Y. Zhu, Q. Qin, F. Xu, F. Fan, Y. Ding, T. Zhang, B.J. Wiley, Z.L. Wang, Size effects on elasticity, yielding, and fracture of silver nanowires: In situ experiments, Phys. Rev. B 85 (4) (2012) 045443. http://dx.doi.org/10.1103/PhysRevB.85.045443.

[28] L. Wang, P. Liu, P. Guan, M. Yang, J. Sun, Y. Cheng, A. Hirata, Z. Zhang, E. Ma, M. Chen, X. Han, In situ atomic-scale observation of continuous and reversible lattice deformation beyond the elastic limit, Nat. Commun. 4 (2013) http://dx.doi.org/10.1038/ncomms3413.

[29] B. Roos, B. Kapelle, G. Richter, C.A. Volkert, Surface dislocation nucleation controlled deformation of Au nanowires, Appl. Phys. Lett. 105 (20) (2014) 201908. http://dx.doi.org/10.1063/1.4902313.

[30] C. Leclere, T.W. Cornelius, Z. Ren, A. Davydok, J.-S. Micha, O. Robach, G. Richter, L. Belliard, O. Thomas, In situ bending of an Au nanowire monitored by micro Laue diffraction, J. Appl. Crystallogr. 48 (1) (2015) 291–296. http://dx.doi.org/10.1107/S1600576715001107.

[31] H. Wu, Molecular dynamics simulation of loading rate and surface effects on the elastic bending behavior of metal nanorod, Comput. Mater. Sci. 31 (3–4) (2004) 287–291. http://dx.doi.org/10.1016/j.commatsci.2004.03.017.

[32] P.A.T. Olsson, S. Melin, C. Persson, Atomistic simulations of tensile and bending properties of single-crystal BCC iron nanobeams, Phys. Rev. B 76 (22) (2007) 224112. http://dx.doi.org/10.1103/PhysRevB.76.224112.

[33] W. Cai, W. Fong, E. Elsen, C. Weinberger, Torsion and bending periodic boundary conditions for modeling the intrinsic strength of nanowires, J. Mech. Phys. Solids 56 (11) (2008) 3242–3258. http://dx.doi.org/10.1016/j.jmps.2008.07.005.

[34] G. Yun, H.S. Park, Surface stress effects on the bending properties of FCC metal nanowires, Phys. Rev. B 79 (19) (2009) 195421. http://dx.doi.org/10.1103/PhysRevB.79.195421.

[35] Z.-J. Wang, C. Liu, Z. Li, T.-Y. Zhang, Size-dependent elastic properties of Au nanowires under bending and tension—Surfaces versus core nonlinearity, J. Appl. Phys. 108 (8) (2010) 083506. http://dx.doi.org/10.1063/1.3493264.

[36] S.K. Deb Nath, S.-G. Kim, On the elastic, elastic–plastic properties of Au nanowires in the range of diameter 1-200 nm, J. Appl. Phys. 112 (12) (2012) 123522. http://dx.doi.org/10.1063/1.4770356.

[37] W. Zhu, H. Wang, W. Yang, Orientation-and microstructure-dependent deformation in metal nanowires under bending, Acta Mater. 60 (20) (2012) 7112–7122. http://dx.doi.org/10.1016/j.actamat.2012.09.018.

[38] H.F. Zhan, Y.T. Gu, Modified beam theories for bending properties of nanowires considering surface/intrinsic effects and axial extension effect, J. Appl. Phys. 111 (8) (2012) 084305. http://dx.doi.org/10.1063/1.3703673.

[39] J.J. Möller, A. Prakash, E. Bitzek, FE2AT—Finite element informed atomistic simulations, Modelling Simul. Mater. Sci. Eng. 21 (2013) 055011. http://dx.doi.org/10.1088/0965-0393/21/5/055011.

[40] X. Tian, J. Cui, C. Zhang, Z. Ma, R. Wan, Q. Zhang, Investigations on the deformation mechanisms of single-crystalline Cu nanowires under bending and torsion, Comput. Mater. Sci. 83 (2014) 250–254. http://dx.doi.org/10.1016/j.commatsci.2013.11.001.

[41] S. Zhang, Microstructure-and surface orientation-dependent mechanical behaviors of Ag nanowires under bending, Comput. Mater. Sci. 95 (2014) 53–62. http://dx.doi.org/10.1016/j.commatsci.2014.07.016.

[42] J.J. Zhang, Y.D. Yan, X. Liu, T. Sun, Y.C. Liang, Influence of coherent twin boundaries on three-point bending of gold nanowires, J. Phys. D: Appl. Phys. 47 (19) (2014) 195301. http://dx.doi.org/10.1088/0022-3727/47/19/195301.

[43] G. Richter, K. Hillerich, D.S. Gianola, R. Mönig, O. Kraft, C.A. Volkert, Ultrahigh strength single crystalline nanowhiskers grown by physical vapor deposition, Nano Lett. 9 (2009) 3048–3052. http://dx.doi.org/10.1021/nl9015107.

[44] L.Y. Chen, G. Richter, J.P. Sullivan, D.S. Gianola, Lattice anharmonicity in defect-free Pd nanowhiskers, Phys. Rev. Lett. 109 (12) (2012) 125503. http://dx.doi.org/10.1103/PhysRevLett.109.125503.

[45] H. Zhan, Y. Gu, C. Yan, P. Yarlagadda, Bending properties of Ag nanowires with pre-existing surface defects, Comput. Mater. Sci. 81 (2014) 45–51. http://dx.doi.org/10.1016/j.commatsci.2013.05.032.

[46] X. Tian, J.Z. Cui, M.Z. Xiang, J.W.Z. Lu, A.Y.T. Leung, V.P. Iu, K.M. Mok, Atomistic simulations on polycrystalline Cu nanowires under tension, bending and torsion loadings, in: AIP Conference Proceedings, American Institute of Physics, 2010, pp. 1315–1320. http://dx.doi.org/10.1063/1.3452094.

[47] E. Bitzek, P. Koskinen, F. Gähler, M. Moseler, P. Gumbsch, Structural relaxation made simple, Phys. Rev. Lett. 97 (17) (2006) 170201. http://dx.doi.org/10.1103/PhysRevLett.97.170201.

[48] W.G. Hoover, Canonical dynamics: equilibrium phase-space distributions, Phys. Rev. A 31 (3) (1985) 1695. http://dx.doi.org/10.1103/PhysRevA.31.1695.

[49] Y. Mishin, M. Mehl, D. Papaconstantopoulos, A. Voter, J. Kress, Structural stability and lattice defects in copper: Ab initio, tight-binding, and embedded-atom calculations, Phys. Rev. B 63 (22) (2001) 224106. http://dx.doi.org/10.1103/PhysRevB.63.224106.

[50] H.S. Park, J.A. Zimmerman, Modeling inelasticity and failure in gold nanowires, Phys. Rev. B 72 (5) (2005) 1–9. http://dx.doi.org/10.1103/PhysRevB.72.054106.

[51] E. Bitzek, F. Gähler, J. Hahn, C. Kohler, G. Krdzalic, J. Roth, C. Rudhart, G. Schaaf, J. Stadler, H.-R. Trebin, Recent developments in IMD: Interactions of covalent and metallic systems, in: E. Krause, W. Jäger (Eds.), High Performance Computing in Science and Engineering 2000, Springer, Heidelberg, 2001.

[52] J. Li, AtomEye: an efficient atomistic configuration viewer, Modelling Simul. Mater. Sci. Eng. 11 (2003) 173–177. http://dx.doi.org/10.1088/0965-0393/11/2/305.

[53] A. Stukowski, Visualization and analysis of atomistic simulation data with OVITO–the open visualization tool, Modelling Simul. Mater. Sci. Eng. 18 (1) (2010) 015012. http://dx.doi.org/10.1088/0965-0393/18/1/015012.

[54] J.D. Honeycutt, H.C. Andersen, Molecular dynamics study of melting and freezing of small Lennard-Jones clusters, J. Phys. Chem. 91 (1987) 4950–4963. http://dx.doi.org/10.1021/j100303a014.

[55] J.A. Zimmerman, C.L. Kelchner, P.A. Klein, J.C. Hamilton, S.M. Foiles, Surface step effects on nanoindentation, Phys. Rev. Lett. 87 (2001) 165507. http://dx.doi.org/10.1103/PhysRevLett.87.165507.

[56] A. Stukowski, V.V. Bulatov, A. Arsenlis, Automated identification and indexing of dislocations in crystal interfaces, Modelling Simul. Mater. Sci. Eng. 20 (8) (2012) 085007. http://dx.doi.org/10.1088/0965-0393/20/8/085007.

[57] M. Brojan, M. Cebron, F. Kosel, Large deflections of non-prismatic nonlinearly elastic cantilever beams subjected to non-uniform continuous load and a concentrated load at the free end, Acta Mech. Sin. 28 (3) (2012) 863–869. http://dx.doi.org/10.1007/s10409-012-0053-3.

[58] J.P. Hirth, J. Lothe, Theory of Dislocations, second ed., John Wiley and Sons, 1982.

[59] R. Fleischer, Cross slip of extended dislocations, Acta Mater. 7 (1959) 134–135. http://dx.doi.org/10.1016/0001-6160(59)90122-1.

[60] E. Bitzek, C. Brandl, P.M. Derlet, H. Van Swygenhoven, Dislocation cross-slip in nanocrystalline FCC metals, Phys. Rev. Lett. 100 (23) (2008) 235501. http://dx.doi.org/10.1103/PhysRevLett.100.235501.

[61] E. Bitzek, P. Gumbsch, Atomistic study of drag, surface and inertial effects on edge dislocations in face-centered cubic metals, Mater. Sci. Eng. A 387–389 (2004) 11–15. http://dx.doi.org/10.1016/j.msea.2004.01.092.

[62] S. Brenner, Tensile strength of whiskers, J. Appl. Phys. 27 (12) (1956) 1484–1491. http://dx.doi.org/10.1063/1.1722294.

[63] G. Cheng, C. Miao, Q. Qin, J. Li, F. Xu, H. Haftbaradaran, E.C. Dickey, H. Gao, Y. Zhu, Large anelasticity and associated energy dissipation in single-crystalline nanowires, Nature Nanotechnol. 10 (2015) 687–691. http://dx.doi.org/10.1038/nnano.2015.135.

[64] Y. Mishin, Handbook of Materials Modeling, Springer, Dordrecht, The Netherlands, 2005, pp. 459–478. (Chapter 2.2 Interatomic potentials for metals).

[65] K. Lee, Large deflections of cantilever beams of non-linear elastic material under a combined loading, Int. J. Non-Linear Mech. 37 (2002) 439–443. http://dx.doi.org/10.1016/S0020-7462(01)00019-1.

[66] M. Brojan, T. Videnic, F. Kosel, Large deflections of nonlinearly elastic non-prismatic cantilever beams made from materials obeying the generalized Ludwick constitutive law, Meccanica 44 (6) (2009) 733–739. http://dx.doi.org/10.1007/s11012-009-9209-z.

[67] J.R. Rice, Dislocation nucleation from a crack tip: An analysis based on the Peierls concept, J. Mech. Phys. Solids 40 (1992) 239–271. http://dx.doi.org/10.1016/S0022-5096(05)80012-2.
[68] J.J. Möller, E. Bitzek, Comparative study of embedded atom potentials for atomistic simulations of fracture in α-iron, Modelling Simul. Mater. Sci. Eng. 22 (4) (2014) 045002. http://dx.doi.org/10.1088/0965-0393/22/4/045002.
[69] M.A. Tschopp, D.L. McDowell, Tension-compression asymmetry in homogeneous dislocation nucleation in single crystal copper, Appl. Phys. Lett. 90 (2007) 121916. http://dx.doi.org/10.1063/1.2715137.
[70] J. Gil Sevillano, Geometrically necessary twins and their associated size effects, Scr. Mater. 59 (2) (2008) 135–138. http://dx.doi.org/10.1016/j.scriptamat.2008.02.052.